Acta Pharmaceutica Sinica B 2022;12(5):2406–2416

Chinese Pharmaceutical Association
Institute of Materia Medica, Chinese Academy of Medical Sciences

Acta Pharmaceutica Sinica B

www.elsevier.com/locate/apsb
www.sciencedirect.com

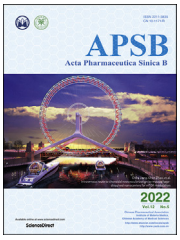

ORIGINAL ARTICLE

A clickable photoaffinity probe of betulinic acid identifies tropomyosin as a target

Pedro Martín-Acosta[a], Qianli Meng[a], John Klimek[a], Ashok P. Reddy[b], Larry David[a,c], Stefanie Kaech Petrie[c,d], Bingbing X. Li[a,*], Xiangshu Xiao[a,c,*]

[a]*Program in Chemical Biology, Department of Chemical Physiology and Biochemistry, Oregon Health & Science University, Portland, OR 97239, USA*
[b]*Proteomics Shared Resource, Oregon Health & Science University, Portland, OR 97239, USA*
[c]*Knight Cancer Institute, Oregon Health & Science University, Portland, OR 97239, USA*
[d]*Department of Neurology, Oregon Health & Science University, Portland, OR 97239, USA*

Received 28 October 2021; received in revised form 25 November 2021; accepted 9 December 2021

KEY WORDS

Betulinic acid;
Cancer;
Diazirine;
Natural product;
Photoaffinity probe;
Tropomyosin

Abstract Target identification of bioactive compounds is important for understanding their mechanisms of action and provides critical insights into their therapeutic utility. While it remains a challenge, unbiased chemoproteomics strategy using clickable photoaffinity probes is a useful and validated approach for target identification. One major limitation of this approach is the efficient synthesis of appropriately substituted clickable photoaffinity probes. Herein, we describe an efficient and consistent method to prepare such probes. We further employed this method to prepare a highly stereo-congested probe based on naturally occurring triterpenoid betulinic acid. With this photoaffinity probe, we identified tropomyosin as a novel target for betulinic acid that can account for the unique biological phenotype on cellular cytoskeleton induced by betulinic acid.

© 2022 Chinese Pharmaceutical Association and Institute of Materia Medica, Chinese Academy of Medical Sciences. Production and hosting by Elsevier B.V. This is an open access article under the CC BY-NC-ND license (http://creativecommons.org/licenses/by-nc-nd/4.0/).

*Corresponding authors. Tel: + 1 503 494 4748.
E-mail addresses: lib@ohsu.edu (Bingbing X. Li), xiaoxi@ohsu.edu (Xiangshu Xiao).

Peer review under responsibility of Chinese Pharmaceutical Association and Institute of Materia Medica, Chinese Academy of Medical Sciences.

https://doi.org/10.1016/j.apsb.2021.12.008
2211-3835 © 2022 Chinese Pharmaceutical Association and Institute of Materia Medica, Chinese Academy of Medical Sciences. Production and hosting by Elsevier B.V. This is an open access article under the CC BY-NC-ND license (http://creativecommons.org/licenses/by-nc-nd/4.0/).

1. Introduction

Naturally occurring substances represent an importance source of our modern-day medicines and biological tools for biomedical research[1]. Prominent examples include taxol, camptothecin and maytansinoids, which are critical leads for current cancer therapies. Betulinic acid (BA, **1**, Fig. 1) is an important natural product that belongs to the pentacyclic lupane-type triterpenoids and has been found in the barks of many species in the plant kingdom[2,3]. Compound **1** showed remarkable anti-melanoma activity *in vitro* and *in vivo* without obvious toxicity[4]. Later, it was found that **1** showed anticancer activity across different cancer types through activating apoptosis[5]. Besides its anticancer activity, compound **1** has also been shown to possess anti-HIV, anti-inflammatory activities in different preclinical models, inhibit melanogenesis through inhibiting cAMP-response element binding protein, and target nuclear lamin B1[3,6–8]. Compound **1** has been reported to be a catalytic inhibitor of topoisomerases[9], an antagonist of peroxisome proliferator-activated receptors (PPARα and γ)[10], an agonist for G-protein coupled receptor TGR5[11,12], and an inhibitor of multiple deubiquitinating enzymes (USP21, USP27x, USP36, USP16)[13]. It is likely that the biological activities of **1** observed in a given biological system are mediated by polypharmacology dictated by the relative expression level of different molecular targets. One particularly striking activity of **1** and its derivatives is their capability to inhibit cancer invasion and modulate actin cytoskeleton. For example, treatment with **1** in fibroblast-like synoviocytes resulted in decreased formation of actin stress fibers[14]. Similar inhibition of actin stress fiber formation was also observed in non-small cell lung cancer cell lines[15]. A number of ring A modified derivatives have also been reported to alter the actin cytoskeleton in prostate cancer cells[16]. Furthermore, other natural pentacyclic triterpenoids related to **1** including betulin, lupeol, oleanolic acid, maslinic acid have all been shown to produce actin cytoskeleton alteration in different cells[17–19]. Despite these dramatic effects on the cytoskeleton in different cells, the underlying molecular mechanism remains elusive.

The challenge in understanding compound **1**'s mechanism of action is a critical bottleneck in unleashing its potential biological and clinical utility. This is true for most of the phenotypic screening assays, where the compounds are assayed against a particular biological phenotype without a prior knowledge of the molecular targets[20,21]. This mechanistic understanding will not only inform biomarker-based clinical utility, but also form the basis for repurposing drugs as well as further mechanistic biological discovery. The centerpiece of understanding the molecular mechanisms of the inhibitors is to identify the targets that the compound can directly bind to, ideally in the unperturbed whole cellular proteome from cultured cells, animal tissues or human clinical samples[22]. Recently, various chemoproteomics-based strategies have been developed to identify the molecular targets of bioactive small molecules[23–25]. Among these, the use of clickable photoaffinity probes is especially appealing and promising to enrich the targets from the whole cellular proteome[26–29]. We recently employed this strategy to identify nuclear lamins as the targets of anticancer pyrroloquinazoline compound LBL1 (Fig. 1)[26,30]. In this case, the clickable photoaffinity probe LBL1-P was synthesized for this purpose (Fig. 1). The diazirine group was expected to generate a reactive carbene species that would covalently crosslink with its direct targets upon UV irradiation at 365 nm[23]. On the other hand, the alkyne group was exploited for next step Cu(I)-catalyzed click reaction with a tagged azide for subsequent target enrichment and/or imaging analysis[31]. Using LBL1-P, we showed that LBL1 targets nuclear lamins in living cells[26,30].

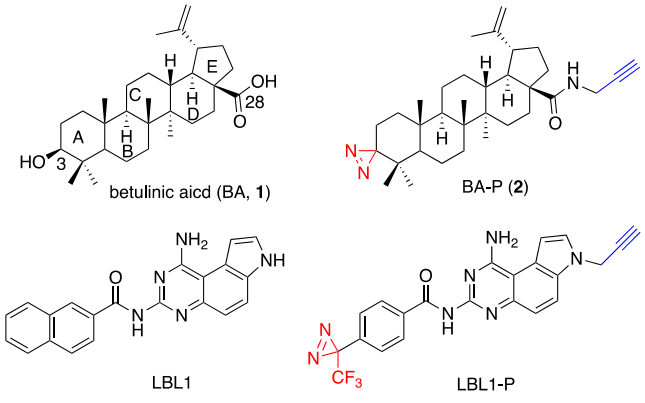

Figure 1 Chemical structures of betulinic acid (BA, **1**) and designed clickable photoaffinity probe BA-P (**2**). The structures of anti-cancer acyl pyrroloquinazoline LBL1 and its corresponding clickable photoaffinity probe LBL1-P are shown.

A chemoproteomics strategy was employed to identify the potential cellular targets of **1**, wherein the clickable photoaffinity label was attached to either C3 through an ester bond or C28 through an amide bond[32]. Interestingly, dozens of proteins were identified from breast cancer MCF-7 cells as possible targets. However, the identified proteins were not overlapping using the two different probes, likely reflecting the potential instability of the ester group in the cellular experiments and different photoaffinity labels used. It is unclear if the identified potential targets can account for compound **1**'s effect on modulating cellular cytoskeleton. Previous structure−activity relationship studies suggested that ring A modification in **1** could dramatically modify its activity in modulating cytoskeleton[16], suggesting that ring A is closely interacting with its potential target contributing to its effect in modulating cytoskeleton. Therefore, it is desirable to design clickable photoaffinity probes that have the photocrosslinking moiety installed in ring A for target identification. Thus, we designed a clickable photoaffinity probe BA-P (**2**) (Fig. 1) to help understand compound **1**'s effect on actin cytoskeleton. The reactive carbene species in ring A generated from **2** would be expected to crosslink with its target for identification *via* the clickable alkyne handle. The overall structure of probe **2** only introduces minimal structural alterations in comparison to that of **1**. In this paper, we developed a novel synthetic method to prepare sterically hindered and synthetically challenging probe **2**. Included in this new method is also the first use of molecular oxygen (O_2) to effect the oxidation of diaziridine to diazirine to inhibit other byproduct formation. We further employed probe **2** to identify tropomyosin as a new target for **1**, potentially accounting for its activity in modulating actin cytoskeleton.

2. Results and discussion

We envisioned that probe **2** could be prepared from its corresponding ketone by the classical diazirine formation method. Being a sterically hindered diazirine and containing a terminal alkyne in **2** are two potential challenges for its synthesis. The synthesis of diazirines typically starts from the corresponding ketones through ketimine formation, diaziridine formation and subsequent oxidation

reaction[33–36]. The reagents for ketimine formation and diaziridine formation are liquid NH_3 and hydroxylamine-*O*-sulfonic acid (NH_2OSO_3H), respectively. A number of reagents have been employed for the oxidation step, which include I_2/Et_3N, freshly prepared Ag_2O[28,33] and MnO_2[37]. While the oxidation step is generally thought to be straightforward (*vide infra*)[33], the first two steps are more troublesome and variable despite their widespread use in the chemical biology community[25,38–40]. This is especially true when other desired functional groups (*e.g.*, terminal alkynes) are present. For example, it was reported that a steroid derivative containing both a ketone and alkyne could not be converted into the corresponding diazirine[33]. Recently, when we attempted to prepare the "minimalist" clickable photocrosslinker **4a** from ketone **3a** (Table 1) following reported conditions[41], we obtained irreproducible and highly variable yields of diazirine **4a** despite our best effort in minimizing experimental variations across the experiments. While we could obtain the desired diazirine **4a** in some instances, we often obtained 0% yield. Furthermore, it has also been reported that the conventional condition for diazirine formation is highly sensitive to steric hindrance. Thus, while α-methyl ketones were suitable substrates, α,α-*gem*-dimethyl ketones were unreactive[33,34].

When we followed the procedure developed in the Yao laboratory[41] to prepare **4a**, we often obtained a large amount of uncharacterizable polar species upon addition of NH_2OSO_3H. We hypothesized that the acidic condition together with the presence of oxygen from the air might cause unusual reactions towards the alkyne group. Therefore, we modified the protocol by conducting the reaction in a sealed tube and carefully blowing inert argon into the solution upon addition of a methanolic solution of NH_2OSO_3H while NH_3 was being evaporated. Furthermore, we decreased the reaction time for the ketimine formation step to 2−3 h. Through these modifications, we were able to obtain the corresponding diaziridine consistently (see Experimental Section). The next step of oxidation of diaziridine to diazirine **4a** was effected smoothly in a basic solution of I_2 using I_2/Et_3N. Unlike the reported condition[41], this improved method resulted in reaction mixtures that were very clean and no column chromatography was needed to purify the diazirine product. Only a simple filtration step through a short silica gel plug was sufficient to deliver the product in a pure form. Encouraged by these results, we investigated if this improved protocol was applicable to other substrates (Table 1). 4-Hydroxy-2-butanone (**3b**) was converted to its corresponding diazirine **4b** in 38% yield using the same protocol. The synthesis of diazirine **4c** from 5-hydroxy-2-pentanone (**3c**) was also successful albeit with a lower yield (22%), which is at least partially due to the presence of a mixture of ketone and cyclic hemiketal in the starting material. Ketone **3d** with a benzene ring was successfully converted into the corresponding diazirine **4d** in 54% yield. Cyclic diazirine **4e** was obtained from its corresponding ketone **3e** in a very good yield (58%). However, this condition was not effective in converting α-hydroxyketone **3f** or aromatic ketone **3g** (Table 1).

Table 1 Synthesis of diazirines from ketones using an improved protocol.

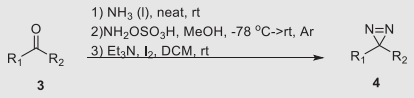

Substrate	Product	Yield
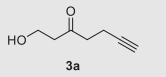 3a	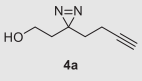 4a	32%
3b	4b	38%
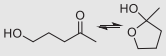 3c	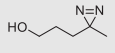 4c	22%
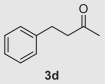 3d	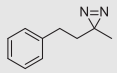 4d	54%
3e	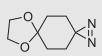 4e	58%
3f	4f	0%
3g	4g	0%

Having established a robust method to synthesize diazirines from the corresponding ketones, we applied this methodology to prepare our designed clickable photoaffinity probe **2** based on **1**. The synthesis of probe **2** was envisioned in 3 steps from commercially available **1** (Scheme 1). Amide **6** was synthesized as previously described[42]. Oxidation of the alcohol in **1** using Jone's reagent provided betulonic acid (**5**) in a high yield (95%). Compound **6** was obtained by the amidation reaction of **5** with propargyl amine using TBTU as the activating agent in DMF (56%). The next key step was to convert the sterically hindered α,α-dimethyl ketone in **6** to its corresponding diazirine **2**. When we employed our optimized protocol for diazirine synthesis, no diaziridine **7** formation was observed. We hypothesized that poor solubility of **6** in liquid NH_3 and MeOH during the reaction might contribute to this failure. Therefore, THF was used as a solvent, where the reaction mixture was a completely homogeneous solution. However, no diaziridine **7** formation was observed in THF. After numerous attempts, we found that a mixture of MeOH/THF (1:1) as the solvent and an extended period of reaction time (6 h) were able to generate the corresponding diaziridine **7** although **6** was not completely soluble under this reaction condition. These results suggest that a protonic solvent is necessary for the diaziridine formation step. The next seemingly trivial oxidation step was proven to be a daunting challenge. Use of I_2/Et_3N in DCM provided an inseparable 1:1 mixture of desired diazirine **2** and vinyl iodide **8** (entry 1, Table 2). Formation of **8** was likely through carbene species **9** *via* newly formed **2**. The generated carbene could react with I_2 to generate carbocation **10** that would be in resonance with iodonium ion **11**. Loss of a proton from **10** or **11** will provide vinyl iodide **8**. This mechanism is reminiscent of Barton's synthesis of vinyl iodides from ketones[43,44]. We attempted to inhibit formation of **8** by performing the reaction in the dark and reducing the molar equivalent of I_2 to be used. Unfortunately, these attempts did not provide pure diazirine **2**.

Other oxidants have also been reported to convert diaziridines to diazirines. Among these, Ag_2O was commonly used[33]. When Ag_2O, pre-formed or generated *in situ*, was used in our case, it failed to yield compound **2** despite disappearance of the diaziridine (entries 2 and 3, Table 2). MnO_2 was the next oxidant to be

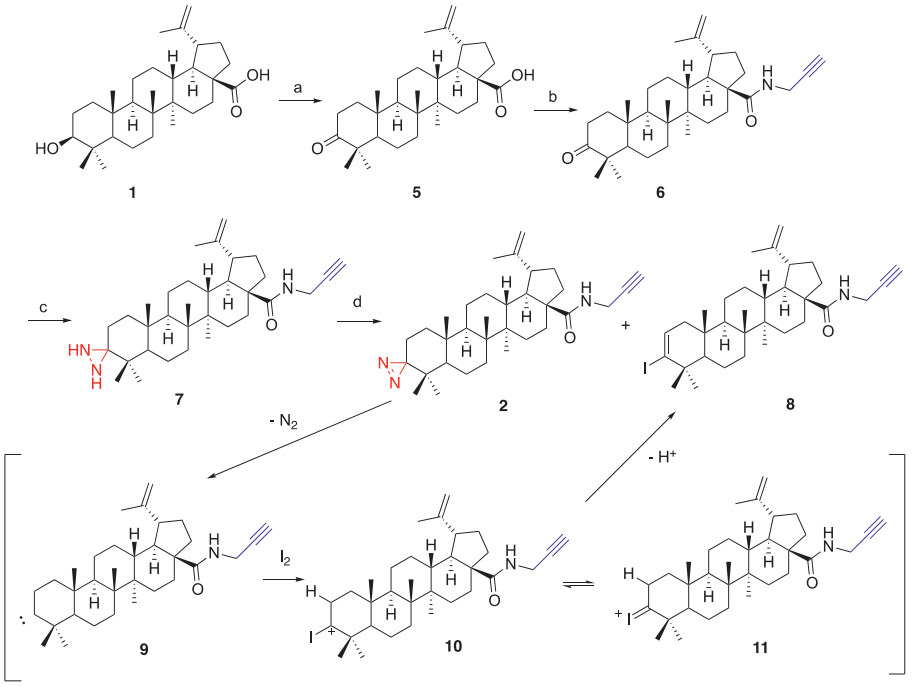

Scheme 1 Synthesis of probe **2**. Reagents and conditions: (a) Jone's reagent, DCM/acetone, 95%; (b) propargylamine, TBTU, DMF, 56%; (c) NH_3, MeOH/THF then NH_2OSO_3H; (d) see Table 2.

investigated[37]. No reaction was observed when diaziridine was reacted with MnO_2 for 24 h (entry 4, Table 2). Encouraged by a recent report that air could promote oxidation of diaziridines in the presence of a base[35], we added KOH and exposed the reaction mixture to air. However, no desired diazirine product was observed either (entry 5, Table 2). On the other hand, when we switched to an O_2 atmosphere under the same reaction condition, the desired diazirine **2** was generated (12%, entry 6, Table 2, Supporting Information Fig. S1). Given the striking difference observed between air and O_2, we speculated that O_2 alone might be sufficient to oxidize diaziridine. Indeed, we found that oxidation of the diaziridine **7** took place under O_2 alone to furnish the expected diazirine **2** in a 11% yield (entry 7, Table 2). To the best of our knowledge, oxidation of diaziridines to diazirines using pure molecular oxygen has not been reported before. While the full scope of this reaction remains to be established, molecular oxygen (O_2) represents a new condition for the diaziridine oxidation with the advantage that this reaction condition could avoid side reactions due to the use of other reagents such as I_2 or strong bases.

Table 2 Oxidation of diaziridine **7** to diazirine **2**.

Entry	Reaction condition	Yield (**2**:**8**)[a]
1	I_2, Et_3N, DCM	14% (1:1)
2	Ag_2O, Et_2O	–[b]
3	$AgNO_3$, NaOH, DCM/MeOH	–[b]
4	MnO_2, Et_2O	NR[c]
5	MnO_2, KOH, air, Et_2O	NR[c]
6	MnO_2, KOH, O_2, Et_2O	12% (1:0)
7	O_2, Et_2O	11% (1:0)

[a]The ratio was determined by ^{1}H NMR.
[b]Diaziridine was decomposed.
[c]No reaction.

With the desired probe **2** in hand, we first evaluated if it retained the biological activity exhibited by **1**. Given the preponderance of evidence of its potential anticancer activity[4,5], we investigated their anti-proliferative activities in breast cancer cell lines. Therefore, breast cancer MDA-MB-468 and MDA-MB-231 cells were treated with different concentrations of **1** and **2** for 72 h. Then the remaining viable cells were quantified using MTT (3-(4,5-dimethylthiazol-2-yl)-2,5-diphenyl tetrazolium bromide) reagent[45]. The concentrations needed to inhibit the cellular growth by 50% were calculated as GI_{50}. As shown in Fig. 2A, compound **2** was ~5-fold less potent (GI_{50} = 12.06 μmol/L) than **1** (GI_{50} = 2.65 μmol/L) in MDA-MB-468 cells. However, in MDA-MB-231 cells, the potency of probe **2** was comparable to that of **1** (GI_{50} = 18.75 *vs* 10.31 μmol/L). These results suggest that probe **2** retains the anticancer activity of **1** and therefore was employed for target identification studies.

To identify the potential molecular targets of **2** in intact cells, we adopted the protocol that we previously developed for target identification with LBL1-P (Fig. 2B)[26,31]. Therefore, we pretreated HEK 293T cells with or without **1** (50 μmol/L) followed by treatment with different concentrations of **2**. The photocrosslinking between **2** and potential cellular targets was initiated by irradiation at 365 nm for 5 min. The resulting cell lysates were then subjected to Cu(I)-catalyzed azide–alkyne cycloaddition (CuAAC) click reaction with tetramethylrhodamine (TMR)-N_3 (Supporting Information Fig. S2). The resulting protein lysates were then analyzed by in-gel fluorescent analysis. As shown in Fig. 2C, probe **2** dose-dependently labeled a few protein bands with the band migrated ~30 kD being most prominent. Importantly, the labeling of this band was competed with an excess of parent compound **1**. The loading across the lanes was comparable based on Coomassie blue staining (Fig. 2D). These results suggest

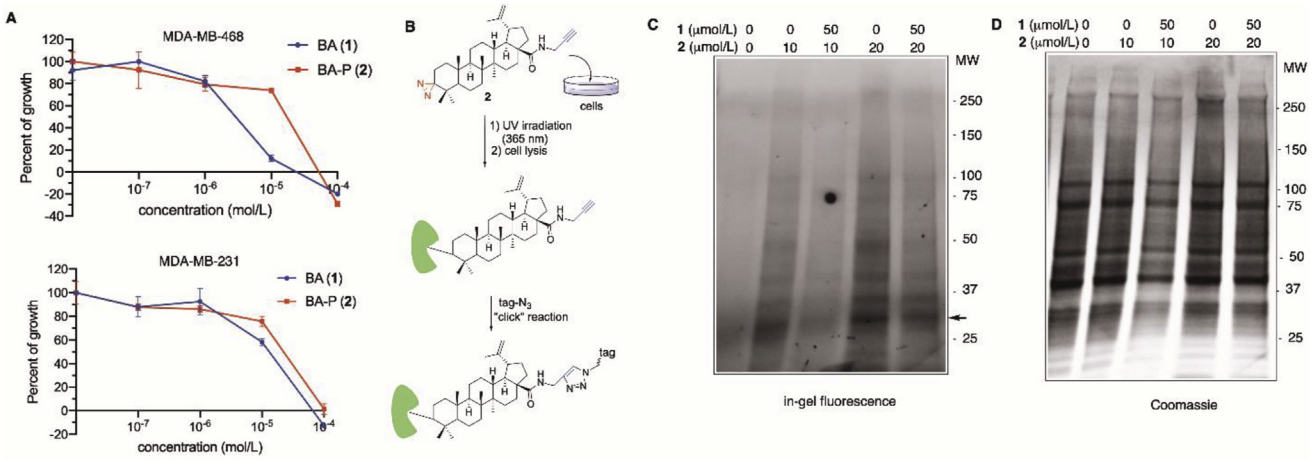

Figure 2 Compound **2** is bioactive and labels cellular targets. (A) Cell growth inhibition activities of **1** and **2** in MDA-MB-468 and MDA-MB-231 cells. The cells were treated with different concentrations of **1** and **2** for 72 h. The viable cells were quantified by the MTT reagent. Negative growth denotes net cell killing effect. (B) A schematic diagram of labeling cellular proteins by **2** in living cells. (C) HEK 293T cells were treated with **1** for 10 min followed by different concentrations of **2** for 30 min. Then the cells were irradiated for 5 min at 365 nm. The lysates were collected and clicked with TMR-azide using Cu(I)-assisted click reaction. The lysates were then resolved on an SDS-PAGE gel for in-gel fluorescence scanning. The MW maker is indicated on the right and the arrow indicates potential cellular targets of **2**. (D) The gel from (C) was stained with Coomassie blue.

that this band was a likely target of **1**. To elucidate the identity of this ~30 kD protein, the crosslinked lysates were subjected to CuAAC with a biotin−N_3 (Fig. S2). The resulting biotinylated proteins were enriched with streptavidin agarose beads. Upon extensive washings and elution with biotin (1 mmol/L) in the presence of 1% SDS, the bound proteins were digested by trypsin, alkylated by iodoacetamide and then subjected to LC–MS/MS analysis. The relative abundance of bound proteins was quantified by label-free spectra counting (Supporting Information Table S1 and Fig. S3). Among the identified proteins, we eliminated the background proteins with high spectra counts in the absence of probe treatment. We further narrowed down the list to those displaying competition by excess of **1**. This analysis gave 3 tropomyosin isoforms (TPM1, TPM2, and TPM3) as the most plausible targets (Fig. 3A and Supporting Information Fig. S4). The spectra counts for these proteins were very low from the sample not treated with probe **2**, but high spectra counts were observed in the sample treated with probe **2** (20 μmol/L). Most importantly, they were competed away by excess of **1** (50 μmol/L) (Fig. 3A). These results suggest that TPMs are putative intracellular targets of **1**.

TPMs are actin-binding proteins and form coiled-coil dimers along the actin filament to regulate actin function and dynamics[46,47]. The human genome encodes four *TPM* genes (*TPM1-4*) and multiple isoforms for each *TPM* gene exist in a cell type-dependent manner through alternative splicing and promoter usage[46]. To confirm if probe **2** could indeed bind to TPM, the cells were treated with **2** followed by UV-irradiation. Then the cell lysates were prepared for click reaction with biotin-N_3. The biotinylated proteins were then purified by streptavidin-agarose precipitation. The bound proteins were analyzed by Western blot. As shown in Fig. 3B, TPM was specifically pulled down from the cells treated with **2**. As a negative control, the abundant cellular protein heat shock protein 90 kD (Hsp90) was tested and it was not precipitated from the cell lysates, suggesting that probe **2** could bind to TPM in living cells.

To further test if **1** was able to bind TPM, we employed cellular thermal shift assay (CETSA)[48]. In this assay, the direct target engagement in the cells was measured by monitoring the difference in protein aggregation upon thermal heating. The cells were treated with 0 or 20 μmol/L of **1** for 3 h. Then the cells were harvested for heating at different temperatures for 3 min. The remaining soluble proteins were extracted for Western blot analysis. In most cases, proteins will aggregate and become insoluble in buffers devoid of detergent, resulting in diminished amount of extractable proteins at higher temperatures[48]. However, in the case of TPM in MDA-MB-468 cells, we did not observe a temperature-dependent decrease of extractable TPM up to 80 °C (Fig. 3C). This surprising finding is consistent with previous observations that TPM from different organisms is heat-stable up to 90 °C[49]. We suggest that this unique thermostability feature will make TPM an appropriate loading control in a typical CETSA experiment, where a loading control is difficult to identify because most proteins are precipitated upon heating. While TPM is heat-stable, we noticed a temperature-dependent increase of extractable TPM from the cells treated with **1** (Fig. 3C), suggesting a direct interaction between **1** and TPM in cells. This increase was likely due to the direct effect of **1** on TPM to modulate its assembly state and/or its interaction with actin filaments. As a control, no changes in the extractability of Hsp10 or P300 proteins were observed (Fig. 3C), suggesting the specificity of the effect on TPM induced by **1**.

To further validate that TPM represents a target of **1**, we performed the in-cell click reaction to localize the signal from probe **2**. MDA-MB-468 cells were treated with **2** for photocrosslinking. Then the cells were subjected to in-cell click reaction with Alexa Fluor™ 555 azide. To enable the comparison with the localization of TPM, the cells were also stained with anti-TPM antibody for indirect immunofluorescence microscopy analysis. We first established the orthogonality of the two channels (Fig. 4A). When the cells were treated with **2** and clicked with Alexa Fluor™ 555

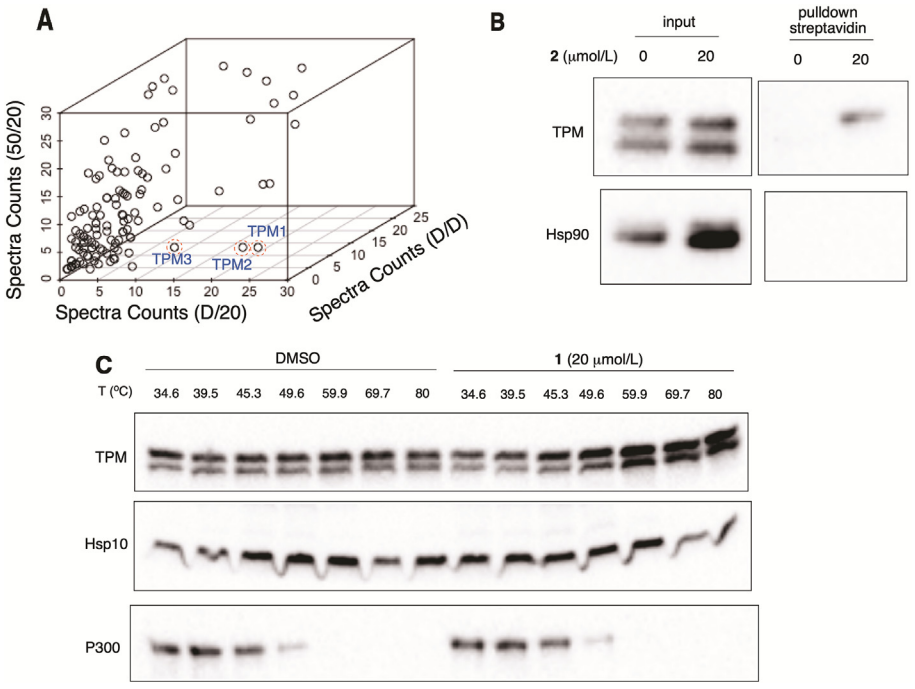

Figure 3 Identification of TPMs as the targets of **1** using clickable photoaffinity probe **2**. (A) Chemoproteomic identification of TPMs as the targets of **2**. HEK 293T cells were treated with 0 or 50 μmol/L of **1** followed by 0 or 20 μmol/L of **2** before photo-irradiation at 365 nm. Then the lysates were clicked with a biotin–N_3 for streptavidin pulldown. The bound proteins were analyzed by LC–MS/MS analysis for identification. The relative abundance of each bound protein was quantified by spectra counting and plotted on each axis. D/D represents the cells treated with DMSO only; D/20 represents the cells treated with 20 μmol/L of **2** whereas 50/20 denotes samples treated with 50 μmol/L of **1** and 20 μmol/L of **2**. (B) Compound **2** binds to TPM in MDA-MB-468 cells. The cells were treated with **2** for photocrosslinking. The lysates were clicked with a biotin–N_3. The biotinylated proteins were precipitated using streptavidin–agarose and the bound proteins were analyzed by Western blot. The two bands observed with anti-TPM is consistent with previous studies showing this antibody recognizes multiple TPM isoforms[46]. (C) Compound **1** binds to TPM in MDA-MB-468 cells as assessed by CETSA. The cells were treated with **1** for 3 h. Then the cells were heated at indicated temperature for 3 min. The remaining soluble proteins were extracted for Western blot analysis using indicated antibodies.

azide, the signal from the click reaction was readily detected under a confocal microscope. No signal was observed in the anti-TPM channel. On the other hand, if the cells were not clicked with Alexa Fluor™ 555 azide but instead stained with anti-TPM, only TPM signal was observed (Fig. 4A). With this orthogonality established, we investigated if the localization of compound **2** overlaps with that of TPM in cells by treating the cells with **2** followed by click reaction with Alexa Fluor™ 555 azide as well as co-staining with anti-TPM. As shown in Fig. 4B, we observed that both **2** and TPM were localized in the cytosol and cellular periphery. No significant staining in the nucleus was observed for either **2** or TPM. We noticed that the signal for TPM staining in the cells was heterogenous with stronger signals in the cellular periphery. However, this was not the case for the signals with **2**. This differential staining for TPM in the cells might be due to different assembly states of TPM, which associates with actin filaments. This partial colocalization and differences in the localization pattern between **2** and TPM might suggest they target different assembly states of TPM in the cells. To further validate that compound **1** could target TPM, we investigated if pretreatment of the cells with **1** would compete with **2** for cellular labeling. Indeed, when the cells were pre-treated with excess **1** before the treatment with **2**, a significant reduction of signal arising from probe **2** was observed (Fig. 4B). When the cells were treated with **1**, we noticed that more TPM signal was distributed to the cellular periphery (Fig. 4B, TPM channel). This change of distribution might be related to the phenomenon we observed in the CETSA assay, where treatment with **1** was accompanied with increased extractability of TPM.

3. Conclusions

In conclusion, we developed an improved method to prepare clickable photoaffinity probes. This improved protocol enables consistent synthesis of diazirines with sensitive functional groups including clickable alkynes. A novel oxidation method to prepare diazirines from diaziridines using O_2 was also developed. To the best of our knowledge, this is the first time to show that molecular oxygen (O_2) can be used for such an oxidation step. This method can avoid the unnecessary byproduct formation derived from the typically used oxidant I_2. We further employed this protocol to synthesize a clickable and stereo-congested photoaffinity probe **2** based on natural product **1** for target identification. TPM was identified as a new target for **1**. It is possible that other less abundant potential targets of **1** (*e.g.*, G-protein coupled receptor

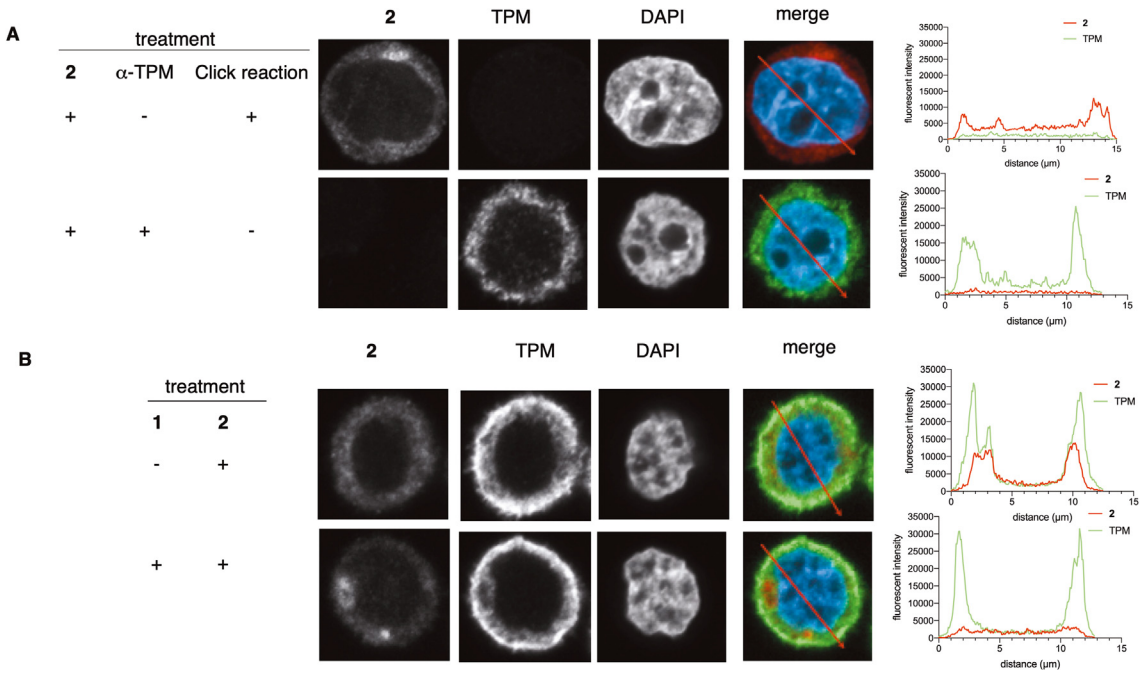

Figure 4 Localization of **2** and TPM in MDA-MB-468 cells. (A) Confocal fluorescent images of **2** and TPM channels. The cells were treated with **2** (1 μmol/L) and were subjected to photoirradiation at 365 nm for 5 min. The cells were fixed and permeabilized for Cu(I)-catalyzed click reaction with Alexa Fluor™ 555 azide (top). The cells from the bottom panel were not subjected to the click reaction, but were instead stained with anti-TPM. The cells were then examined under a confocal microscope. (B) Compound **1** competed with **2** for labelling in cells. The cells were treated with **1** (0 or 10 μmol/L) and **2** (1 μmol/L). Then the cells were processed in the same way as in (A). The cells were also stained with anti-TPM. DAPI was used to stain nucleus. The fluorescent intensity profile for **2** and TPM along the indicated arrow is shown on the right panel.

TGR5[11]) were not identified using probe **2** or not expressed in the cells used in this study. While the other targets identified using different photoaffinity probes may also be relevant targets[32], our identification of TPM as a new target for **1** using probe **2** further highlights the importance of the position of photocrosslinking group in a probe for target identification. This is even more critical for compounds with polypharmacology to comprehensively understand their biological activities. Given the potential roles of **1** in regulating actin cytoskeleton in different cell types, the identification of TPM as a target of **1** provides a potential mechanism to account for this unique effect. This molecular understanding shall further drive the development of **1** and other structurally related natural products into potential cancer therapeutics.

4. Experimental

4.1. Chemistry

4.1.1. General

Anhydrous solvents were used for reaction and were either obtained directly from vendors or purified from sodium/benzophenone distillation (THF) or CaH_2 distillation (DCM). Melting points were determined in capillary tubes using Mel-Temp and are uncorrected. All ^1H and ^{13}C NMR spectra were obtained in a Bruker Avance 400 MHz spectrometer using $CDCl_3$ or DMSO-d_6 as the solvent and the chemical shifts of the residual $CHCl_3$ (δ 7.26) or DMSO (δ 2.50) were taken as reference. Chemical shifts (δ) are reported in parts per million (ppm), and the signals are described as brs (broad singlet), d (doublet), dd (doublet of doublet), td (triplet of doublet), m (multiplet), q (quartet), s (singlet) and t (triplet). Coupling constants (J values) are given in Hz. Silica gel flash chromatography was performed using 230−400 mesh silica gel (EMD). All reactions were monitored using thin-layer chromatography (TLC) on silica gel plates (EMD). Yields were of purified compounds. The mass spectra were obtained from an Advion Plate Express Compact Mass Spectrometer (Advion) with electrospray operated either in positive or negative mode.

4.1.2. Synthesis

*4.1.2.1. Compound **4a**.* Anhydrous ammonia (~5 mL) was condensed into a sealed tube at −78 °C in an acetone-dry ice bath. Compound **3a** (200 mg, 1.6 mmol) was added at −78 °C, and the mixture was stirred at room temperature for 2 h. The solution was cooled to −78 °C, and a solution of hydroxylamine-*O*-sulfonic acid (206 mg, 1.8 mmol) in methanol (2 mL) was added in a dropwise manner. Dry ice refill was discontinued, and the reaction was allowed to gradually warm to room temperature. The seal was removed to allow the remaining ammonia to evaporate overnight, and a slow Ar flow was running overnight on top of the solution. The resulting slurry was filtered and the filter cake was washed with several portions of methanol (3 × 5 mL). The combined solution was evaporated under reduced pressure. The residue of the diaziridine derivative was dissolved in dichloromethane (5 mL) and treated with triethylamine (276 μL, 2.0 mmol) at room temperature. A solution of iodine (301 mg, 1.2 mmol) in dichloromethane (1 mL) was slowly added with stirring until the appearance of a persistent orange-brown coloration. The mixture was diluted with 30 mL DCM, and washed with 50 mL sat. Na_2SO_3 (aq), 50 mL 1 mol/L HCl (aq) and 50 mL sat. NaCl (aq).

All solvents were evaporated under reduced pressure to give compound **4a** (68 mg, 31%) as a brown oil: ^{1}H NMR (400 MHz, $CDCl_3$) δ 3.44 (t, J = 6.2 Hz, 2H), 2.12 (s, 1H), 2.04−1.94 (m, 3 H), 1.69−1.62 (m, 4H). ^{13}C NMR (101 MHz, $CDCl_3$) δ 82.92, 69.30, 57.25, 35.52, 32.63, 26.69, 13.26.

*4.1.2.2. Betulonic acid or (1R,3aS,5aR,5bR,11aR)-5a,5b,8,8,11a-pentamethyl-9-oxo-1-(prop-1-en-2-yl)icosahydro-3aH-cyclopenta[a]chrysene-3a-carboxylic acid (**5**).* Betulinic acid **1** (500 mg, 1.1 mmol) was dissolved in DCM/acetone (1:1, 24 mL) and placed at 0 °C. Jones reagent (1.0 mL) was slowly added and the reaction mixture was stirred at r.t. for 15 min. MeOH (5 mL) was added and the reaction mixture was stirred for another 10 min. DCM (20 mL) was added and the reaction mixture was washed with water (2 × 20 mL), brine (30 mL) and dried over anhydrous Na_2SO_4. The crude was purified by column chromatography in silica gel eluting with hexanes/EA 4:1 affording the product **5** (470 mg, 95%) as a white solid. Mp.: >220 °C. ^{1}H NMR (400 MHz, $CDCl_3$) δ 11.09 (brs, 1H), 4.74 (s, 1H), 4.61 (s, 1H), 3.01 (td, J = 10.7, 4.6 Hz, 1H), 2.55−2.34 (m, 2H), 2.33−2.13 (m, 2H), 2.12−1.79 (m, 4H), 1.74−1.59 (m, 5H), 1.51−1.24 (m, 14H), 1.07 (s, 3H), 1.01 (s, 3H), 0.99 (s, 3H), 0.97 (s, 3H), 0.92 (s, 3H). ^{13}C NMR (100 MHz, $CDCl_3$) δ 218.38, 182.40, 150.50, 109.96, 56.59, 55.12, 50.03, 49.38, 47.52, 47.08, 42.68, 40.82, 39.79, 38.71, 37.23, 37.11, 34.31, 33.79, 32.29, 30.74, 29.87, 26.83, 25.68, 21.56, 21.18, 19.81, 19.56, 16.14, 16.01, 14.81. ESI-MS: Calcd. for $C_{30}H_{46}O_3$ $[M–H]^-$ 453.3, Found 453.1.

*4.1.2.3. (1R,3aS,5aR,5bR,11aR)-5a,5b,8,8,11a-Pentamethyl-9-oxo-1-(prop-1-en-2-yl)-N-(prop-2-yn-1-yl)icosahydro-3aH-cyclopenta[a]chrysene-3a-carboxamide (**6**) and 1H-benzo[d][1,2,3]triazol-1-yl (1R,3aS,5aR,5bR,11aR)-5a,5b,8,8,11a-pentamethyl-9-oxo-1-(prop-1-en-2-yl)icosahydro-3aH-cyclopenta[a]chrysene-3a-carboxylate (**6a**).* Betulonic acid **5** (370 mg, 0.81 mmol) was dissolved in dry DMF (3 mL) and placed at 0 °C. DIPEA (282.2 μL, 1.62 mmol, 2 equiv) and TBTU (286.1 mg, 0.89 mmol, 1.1 equiv) were added and the reaction mixture was stirred at 0 °C for 30 min. Propargyl amine (91.54 mg, 1.62 mmol, 2 equiv) was added and the reaction mixture was stirred for overnight at r.t. The reaction mixture was treated with a saturated solution of $NaHCO_3$ (10 mL) and extracted with DCM (3 × 10 mL). The combined organic layers were washed with brine (10 mL) and dried over anhydrous Na_2SO_4. The crude was purified by column chromatography in silica gel eluting with hexane/EA (9:1) affording the products **6** (222.5 mg, 56%) and **6a** (117.7 mg, 25%) as white solids.

6: mp 178−180 °C. ^{1}H NMR (400 MHz, $CDCl_3$) δ 5.81−5.64 (m, 1H), 4.73 (s, 1H), 4.59 (s, 1 H), 4.08 (ddd, J = 17.5, 5.0, 2.1 Hz, 1H), 3.97 (ddd, J = 17.5, 4.9, 2.3 Hz, 1H), 3.13 (td, J = 11.0, 4.2 Hz, 1H), 2.56−2.31 (m, 3H), 2.20 (t, J = 1.9 Hz, 1H), 2.07−1.85 (m, 3H), 1.71−1.22 (m, 21H), 1.06 (s, 3H), 1.01 (s, 3H), 0.97 (s, 6H), 0.91 (s, 3H). ^{13}C NMR (101 MHz, $CDCl_3$) δ 218.15, 175.84, 150.75, 109.47, 80.14, 71.12, 55.64, 55.04, 50.13, 50.01, 47.34, 46.66, 42.52, 40.75, 39.65, 38.09, 37.82, 36.93, 34.16, 33.71, 33.57, 30.79, 29.38, 29.00, 26.60, 25.62, 21.44, 21.03, 19.65, 19.50, 15.97, 15.94, 14.58. ESI-MS: Calcd. for $C_{33}H_{49}NO_3$ $[M–H]^-$ 490.4, Found 490.0.

6a: ^{1}H NMR (400 MHz, $CDCl_3$) δ 8.09 (d, J = 8.4 Hz, 1H), 7.56 (t, J = 7.9 Hz, 1H), 7.43 (t, J = 7.7 Hz, 1H), 7.37 (d, J = 8.3 Hz, 1H), 4.74 (s, 1H), 4.65 (s, 1H), 2.96 (td, J = 11.1, 5.1 Hz, 1 H), 2.69−2.58 (m, 1H), 2.56−2.31 (m, 3H), 2.31−2.18 (m, 1H), 2.18−2.03 (m, 1H), 1.92−1.67 (m, 9 H), 1.54−1.27 (m, 12H), 1.09 (s, 3H), 1.06 (s, 3H), 1.03 (s, 6H), 0.93 (s, 3H). ESI-MS: Calcd. for $C_{36}H_{49}N_3O_3$ $[M+H]^+$ 572.4, Found 572.3.

*4.1.2.4. (1R,3aS,5aR,5bR,11aR)-5a,5b,8,8,11a-Pentamethyl-1-(prop-1-en-2-yl)-N-(prop-2-yn-1-yl)-2,3,4,5,5a,5b,6,7,7a,8,10,11,11a,11b,12,13,13a,13b-octadecahydrospiro[cyclopenta[a]chrysene-9,3′-diazirine]-3a(1H)-carboxamide (**2**).* NH_3 (g) was condensed into a high-pressure tube at −78 °C. Compound **6** (50 mg, 0.1 mmol) was suspended in MeOH/THF (1 mL, 1:1) and added to the liquid ammonia (~5 mL). The tube was sealed and the reaction mixture was stirred at r.t. for 6 h. The reaction mixture was cooled to −78 °C and NH_2OSO_3H (13.8 mg, 0.12 mmol, 1.2 equiv) dissolved in MeOH (1 mL) was slowly added under argon. The reaction mixture was slowly warmed up to room temperature while ammonia was evaporated under a stream of argon. The remaining reaction mixture was stirred overnight at room temperature. The reaction mixture was filtered and the solid was washed with MeOH (5 mL) and DCM (5 mL). The filtrate was concentrated under vacuum. The residue was dissolved in Et_2O (3 mL) and stirred at r.t. under O_2 atmosphere in the dark until disappearance of the starting material (3 h). The solvent was removed under reduced pressure and the crude was purified by column chromatography on silica gel eluting with Hexanes/EtOAc (9:1 to 4:1) to yield 3.6 mg of compound **2** (11%) as a colorless oil and recovered 20.3 mg of the starting material **6**.

2: ^{1}H NMR (400 MHz, $CDCl_3$) δ 5.73 (t, J = 5.1 Hz, 1H), 4.74 (s, 1H), 4.60 (s, 1H), 4.09 (ddd, J = 18.3, 4.7, 2.4 Hz, 1H), 3.97 (ddd, J = 18.7, 5.1, 2.5 Hz, 1H), 3.14 (td, J = 11.1, 3.9 Hz, 1H), 2.44 (td, J = 12.0, 3.5 Hz, 1H), 2.21 (t, J = 2.4 Hz, 1H), 2.05−1.90 (m, 3H), 1.79−1.73 (m, 2H), 1.69 (s, 3H), 1.64−1.56 (m, 4H), 1.47−1.37 (m, 9H), 1.21−1.14 (m, 4H), 1.00 (s, 3H), 0.97 (s, 3H), 0.95 (s, 3H), 0.90 (s, 3H), 0.24−0.20 (m, 1H), 0.17 (s, 3H). ^{13}C NMR (101 MHz, $CDCl_3$) δ 175.87, 150.82, 109.50, 80.14, 71.18, 55.71, 55.66, 50.33, 50.13, 46.72, 42.55, 40.85, 38.13, 37.74, 37.41, 37.29, 36.33, 34.09, 33.63, 30.78, 29.72, 29.36, 29.01, 26.59, 25.64, 25.57, 20.94, 19.48, 19.18, 18.86, 16.24, 15.56, 14.63. ESI-MS: Calcd. for $C_{33}H_{49}N_3O$ $[M–H]^-$ 502.4, Found 502.1.

4.2. Biology

4.2.1. Cell culture

MDA-MB-468 and MDA-MB-231 were obtained from Developmental Therapeutics Program at the National Cancer Institute. HEK293T cells were obtained from ATCC. All the cells were authenticated by STR profiling using Promega 10 GenePrint assay. The cells were cultured in Dulbecco's Modified Eagle Medium (DMEM) supplemented with 10% fetal bovine serum and non-essential amino acids in a humidified incubator at 37 °C with 5% CO_2. The cells were used until passage 50. The following antibodies were used: anti-TPM (Sigma, cat #T2780), anti-Hsp10 (Bethyl laboratories, cat # A304-842A-M), anti-Hsp90 (cat # 4874) and anti-P300 (cat # 54,062) (Cell Signaling Technology). Secondary antibodies were from Jackson ImmunoResearch Laboratories.

4.2.2. MTT assay

The cells were plated into 96-well plates on the day before they were treated. Then the cells were treated with different compounds at different concentrations for 72 h. At the end of drug

treatment, the cells were incubated with MTT reagent at 0.5 mg/mL in tissue culture media for 3 h. Then the media were removed and the reduced purple formazan was dissolved in DMSO. The absorbance values at 560 nm were recorded using i3 multimode plate reader (Molecular Devices). The percent of growth is defined as $(A_{treated}-A_{initial})/(A_{control}-A_{initial}) \times 100$, where $A_{treated}$ represents absorbance in wells treated with a compound, $A_{initial}$ represents the absorbance at time 0, and $A_{control}$ denotes media-treated cells. The GI_{50} values were calculated by non-linear regression analysis in Prism 8.0.

4.2.3. *Photocrosslinking and click chemistry for gel analysis*

HEK293T cells in 6-well plates were washed once with PBS. Then the cells were treated with indicated concentration of **1** for 10 min in PBS, when different concentrations of 2 were added. The cells were incubated for another 30 min at 37 °C. The cells were then irradiated at 365 nm for 5 min using UV crosslinker (FB-UVXL-1000, Fisher Scientific) at 4 °C. The cells were harvested and centrifuged at 8000 rpm for 5 min at 4 °C. The cell pellets were washed once with cold PBS. The washed cell pellets were lysed in 1% SDS/PBS with brief sonications. Then 10 μg of the cleared cell lysates were subjected to click reaction with TMR-N_3 (50 μmol/L) in the presence of TCEP (1 mmol/L), TBTA (100 μmol/L) and $CuSO_4$ (1 mmol/L). The click reaction mixture was incubated with shaking in the dark at room temperature for 1.5 h. The reaction mixture was then loaded onto a 4%−20% SDS-PAGE gel electrophoresis. The gel was then visualized using fluorescence gel scanning with ChemiDoc MP (Bio-Rad). After fluorescence gel scanning, the gel was stained with Coomassie brilliant blue staining solution.

For streptavidin pulldown analysis by Western blot, MDA-MB-468 cells were treated with indicated concentration of **2** for 30 min in PBS. Then the cells were treated as above. After the cells were lysed, equal amount of cell lysates was clicked with biotin–N_3 (50 μmol/L) using the same click reaction mixture as above. After click reaction, the mixture was mixed with 1 volume of methanol and $^1/_4$ volume of $CHCl_3$. The mixture was vortexed and centrifuged at 8000×*g* for 10 min. The protein solid was saved and washed with 3 times with MeOH:$CHCl_3$ (1:1). Then washed protein solids were resuspended in 1 volume of MeOH and $^1/_4$ volume of $CHCl_3$. The mixture was centrifuged at 14,000 rpm for 10 min at room temperature. The solid was redissolved in 1% SDS/PBS with sonication. Any undissolved material was discarded. The protein solution was diluted 10 × with PBS. Streptavidin-agarose was added to the protein solution and the mixture was tumbled for 2 h at room temperature. The beads were collected by centrifuge and further washed with 1% SDS/PBS (3 ×) and PBS (6 ×). The bound proteins were eluted in 1 × SDS-PAGE sample buffer with 1 mm/L biotin upon heating at 95 °C for 5 min. The eluted proteins were analyzed by Western blot analysis.

4.2.4. *Photocrosslinking and click chemistry for LC–MS/MS analysis*

HEK293T cells (3 × 15-cm plates/condition) were treated with indicated compounds for 10 min in PBS followed by the addition of compound 2 for 30 min. Then the cells were processed in the same way as above for Western blot analysis the following exception. The bound proteins were eluted with 1% SDS/PBS with 1 mol/L biotin upon heating at 95 °C for 5 min. The eluted proteins were then subjected to proteomics analysis as described below.

4.2.5. *Protein LC–MS/MS*

Affinity purified proteins from above were dried by vacuum centrifugation, redissolved in 20 μL of SDS-PAGE sample buffer, applied to wells of a NuPAGE 10% Bis-Tris SDS-PAGE gel (NP0301BOX), electrophoresed for 6 min at 200 V, and stained for 30 min with Imperial Blue protein stain (Catalog No. 24615; Thermo Scientific). The gel was then rinsed in water and the entire top 1 cm of each lane containing proteins was excised, cut into 1 mm pieces, reduced/alkylated, and digested with trypsin for 1 h at 50 °C in the presence of 0.01% ProteaseMax detergent using the method recommended from the manufacturer (ProMega). Recovered peptides were then filtered using 0.22 μm Millipore Ultrafree-CL centrifugal filters, filtrate dried by vacuum centrifugation then dissolved in 20 μL of 5% formic acid in preparation for mass spectrometric analysis.

Each digest was then chromatographically separated using a Dionex RSLC UHPLC system and delivered to a Q-Exactive HF mass spectrometer (Thermo Scientific) using electrospray ionization with a Nano Flex Ion Spray Source fitted with a 20 μm stainless steel nano-bore emitter spray tip and 1.0 kV source voltage. Xcalibur version 4.0 was used to control the system. Samples were applied at 10 μL/min to a Symmetry C18 trap cartridge (Waters) for 5 min, then switched onto a 75 μm × 250 mm NanoAcquity BEH 130 C18 column with 1.7 μm particles (Waters) using mobile phases water (A) and acetonitrile (B) containing 0.1% formic acid, 7.5%−30% acetonitrile gradient over 60 min, and 300 nL/min flow rate. Survey mass spectra were acquired over *m/z* 375−1400 at 120,000 resolution (*m/z* 200) and data-dependent acquisition selected the top 10 most abundant precursor ions for tandem mass spectrometry by HCD fragmentation using an isolation width of 1.2 *m/z*, normalized collision energy of 30, and a resolution of 30,000. Dynamic exclusion was set to auto, charge state for MS/MS +2 to +7, maximum ion time 100 ms, minimum AGC target of 3×10^6 in MS1 mode and 5×10^3 in MS2 mode.

Comet (v. 2016.01, rev. 3)[50] was used to search 64,782 MS2 spectra against a UniProt human Swiss-Prot protein FASTA collection (v2020.06 with 20,366 sequences). The FASTA file was augmented with 179 common contaminant sequences and concatenated sequence-reversed entries of all proteins (to estimate error thresholds). The database processing used Python scripts available at https://github.com/pwilmart/fasta_utilities.git and Comet results processing used the PAW pipeline[51] from https://github.com/pwilmart/PAW_pipeline.git. Comet searches for all samples were performed with trypsin enzyme specificity (maximum of two missed cleavages) with monoisotopic parent ion mass tolerance set to 1.25 Da and monoisotopic fragment ion mass tolerance set at 0.02 Da. A static modification of +57.02146 Da added to all cysteine residues and a variable modification of +15.9949 Da on methionine residues. Comet scores were combined into linear discriminant function scores[51,52], and discriminant score histograms created separately for each peptide charge state (2+, 3+, and 4+). Separate histograms were created for peptide-spectrum-matches (PSMs) to forward sequences and for matches to reversed sequences for all peptides of seven amino acids or longer. The score histograms of reversed matches were used to estimate PSM false discovery rates (FDR) and set score thresholds for each PSM class at 2%. There were 8887 PSMs passing thresholds and mapped to proteins using basic and extended parsimony principles. There were 387 proteins (including contaminants and decoy proteins) inferred using a two distinct peptide sequences per protein requirement. Only one

decoy protein was reported in the final list. The data were plotted using Scatterplot3d in RStudio.

4.2.6. *CETSA experiment*

MDA-MB-468 cells in a 10-cm plate were treated with indicated concentrations of the drug for 3 h at 37 °C. Then the cells were collected and washed with cold PBS (Na_2HPO_4 (4.3 mmol/L), KH_2PO_4 (1.4 mmol/L), KCl (2.7 mmol/L), NaCl (137 mmol/L), pH 7.4). The cells were resuspended in 80 μL of PBS and 10 μL of the cell suspension was aliquoted into PCR tubes. The samples were heated at indicated temperature for 3 min followed by 25 °C for 3 min in a PCR thermal cycler. Then 20 μL HBS (20 mmol/L HEPES, 250 mmol/L NaCl, pH 8.0) supplemented with protease inhibitor cocktail (Roche) and 1 mmol/L PMSF was added to the cell suspension, which was then subjected to 3 cycles of freezing/thawing in liquid nitrogen. The lysates were centrifuged at 14,000 rpm for 15 min at 4 °C and supernatant was analyzed by Western blot with indicated antibodies.

4.2.7. *Western blot analysis*

The samples were boiled at 95 °C for 5 min. After centrifugation, the samples were loaded onto 4%−20% SDS-PAGE gel (Bio-Rad) for separation. The gel was then transferred to nitrocellulose membrane by electroblot. The membranes were blocked with 5% nonfat dry milk in TBST (Tris (50 mmol/L), NaCl (150 mmol/L), Tween-20 (0.1%), pH 7.5). After blocking, the membranes were incubated with indicated primary antibodies for overnight at 4 °C. The membrane was washed 3 × using TBST and incubated with secondary HRP-conjugated antibodies for 1 h at room temperature. After washing in TBST for 3 times, the membranes were imaged using ChemiDoc^{MP} (Bio-Rad).

4.2.8. *In-cell click reaction and immunofluorescence*

Cover slips were precoated with poly-lysine (Sigma) solution for overnight. MDA-MB-468 cells were allowed to grow on the cover slips the day before the experiment treatment. The cells were then treated with indicated concentrations of compounds in PBS for 30 min before the addition of compound **2** for 20 min. The cells were cooled to 4 °C and UV-irradiated at 365 nm for 5 min. The cells were then fixed with 3.7% formaldehyde and permeabilized with 0.5% Triton X-100. After fixing and permeabilization, the cells were washed with 3% BSA in PBS. Then the click reaction was initiated using Click-iT® Cell reaction cocktail (Thermo Fisher) supplemented with Alexa Fluor™ 555-N_3 (Thermo Fisher) for 30 min at room temperature. Then the cells were washed with 3% BSA in PBS before being incubated with anti-TPM (1:3000, 1.4 μg/mL) overnight. The cells were then incubated with Alexa Fluor 488 donkey anti-mouse secondary antibody (1:1000, 1.5 μg/mL) for 1 h at room temperature. The cell nucleus was stained with DAPI (300 nmol/L) for 10 min at room temperature. The coverslips were then mounted in ProLong Gold AntiFade Reagent without DAPI (Thermo Fisher). Optically sectioned images were acquired on a ZEISS LSM 900 or LSM 980 laser-scanning confocal microscope using a 63 × 1.4 Plan Apochromat lens and light path and optimal resolution settings suggested by the manufacturer.

Acknowledgments

This work was made possible partially by the financial supports from the National Institutes of Health R01 CA197513 (XX), R01 GM122820 (XX) and R21EB028425 (BXL), USA. We thank the OHSU Massively Parallel Sequencing Shared Resources Core for the STR profiling assays to authenticate the cell lines. Mass spectrometric analysis was performed by the OHSU Proteomics Shared Resource with partial support from NIH core grants P30EY010572, P30CA069533, and S10RR025571, USA.

Author contributions

Pedro Martin-Acosta, Qianli Meng, Bingbing X. Li and Xiangshu Xiao designed and performed experiments; John Klimek, Ashok P. Reddy and Larry David conducted and analyzed the proteomics experiment; Stefanie Kaech Petrie contributed analytical tools and analyzed the data; Pedro Martin-Acosta, Qianli Meng, Bingbing X. Li and Xiangshu Xiao analyzed and interpreted the results; Bingbing X. Li and Xiangshu Xiao supervised the research; Xiangshu Xiao conceived the project. Pedro Martin-Acosta, Qianli Meng, Bingbing X. Li and Xiangshu Xiao wrote the manuscript with inputs from all authors. All authors have given approval to the final version of the manuscript.

Conflicts of interest

The authors declare no conflicts of interest.

Appendix A. Supporting information

Supporting information to this article can be found online at https://doi.org/10.1016/j.apsb.2021.12.008.

References

1. Newman DJ, Cragg GM. Natural products as sources of new drugs from 1981 to 2014. *J Nat Prod* 2016;**79**:629−61.
2. Robertson A, Soliman G, Owen EC. Polyterpenoid compouds. Part I. Betulinic acid from *Cornus florida*, L. *J Chem Soc* 1939:1267−73.
3. Cichewicz RH, Kouzi SA. Chemistry, biological activity, and chemotherapeutic potential of betulinic acid for the prevention and treatment of cancer and HIV infection. *Med Res Rev* 2004;**24**:90−114.
4. Pisha E, Chai H, Lee IS, Chagwedera TE, Farnsworth NR, Cordell GA, et al. Discovery of betulinic acid as a selective inhibitor of human melanoma that functions by induction of apoptosis. *Nat Med* 1995;**1**:1046−51.
5. Fulda S, Friesen C, Los M, Scaffidi C, Mier W, Benedict M, et al. Betulinic acid triggers CD95 (APO-1/Fas)- and p53-independent apoptosis *via* activation of caspases in neuroectodermal tumors. *Cancer Res* 1997;**57**:4956−64.
6. Li L, Du Y, Kong X, Li Z, Jia Z, Cui J, et al. Lamin b1 is a novel therapeutic target of betulinic acid in pancreatic cancer. *Clin Cancer Res* 2013;**19**:4651−61.
7. Jin KS, Oh YN, Hyun SK, Kwon HJ, Kim BW. Betulinic acid isolated from vitis amurensis root inhibits 3-isobutyl-L-methylxanthine induced melanogenesis *via* the regulation of MEK/ERK and PI3K/AKT pathways in b16f10 cells. *Food Chem Toxicol* 2014;**68**:38−43.
8. Li H, Sun J, Xiao S, Zhang L, Zhou D. Triterpenoid-mediated inhibition of virus-host interaction: is now the time for discovering viral entry/release inhibitors from nature?. *J Med Chem* 2020;**63**:15371−88.
9. Syrovets T, Büchele B, Gedig E, Slupsky JR, Simmet T. Acetyl-boswellic acids are novel catalytic inhibitors of human topoisomerases I and IIalpha. *Mol Pharmacol* 2000;**58**:71−81.
10. Brusotti G, Montanari R, Capelli D, Cattaneo G, Laghezza A, Tortorella P, et al. Betulinic acid is a PPARγ antagonist that improves glucose uptake, promotes osteogenesis and inhibits adipogenesis. *Sci Rep* 2017;**7**:5777.

11. Lo SH, Cheng KC, Li YX, Chang CH, Cheng JT, Lee KS. Development of betulinic acid as an agonist of TGR5 receptor using a new *in vitro* assay. *Drug Des Devel Ther* 2016;**10**:2669−76.
12. Yun Y, Zhang C, Guo S, Liang X, Lan Y, Wang M, et al. Identification of betulinic acid derivatives as potent TGR5 agonists with antidiabetic effects *via* humanized $TGR5^{H88Y}$ mutant mice. *J Med Chem* 2021;**64**:12181−99.
13. de Las Pozas A, Reiner T, De Cesare V, Trost M, Perez-Stable C. Inhibiting multiple deubiquitinases to reduce androgen receptor expression in prostate cancer cells. *Sci Rep* 2018;**8**:13146.
14. Li N, Gong Z, Li X, Ma Q, Wu M, Liu D, et al. Betulinic acid inhibits the migration and invasion of fibroblast-like synoviocytes from patients with rheumatoid arthritis. *Int Immunopharmacol* 2019;**67**:186−93.
15. Hsu TI, Chen YJ, Hung CY, Wang YC, Lin SJ, Su WC, et al. A novel derivative of betulinic acid, SYK023, suppresses lung cancer growth and malignancy. *Oncotarget* 2015;**6**:13671−87.
16. Härmä V, Haavikko R, Virtanen J, Ahonen I, Schukov HP, Alakurtti S, et al. Optimization of invasion-specific effects of betulin derivatives on prostate cancer cells through lead development. *PLoS One* 2015;**10**:e0126111.
17. Ebeling S, Naumann K, Pollok S, Wardecki T, Vidal YSS, Nascimento JM, et al. From a traditional medicinal plant to a rational drug: understanding the clinically proven wound healing efficacy of birch bark extract. *PLoS One* 2014;**9**:e86147.
18. Hata K, Hori K, Murata J, Takahashi S. Remodeling of actin cytoskeleton in lupeol-induced B16 2F2 cell differentiation. *J Biochem* 2005;**138**:467−72.
19. Martín R, Carvalho-Tavares J, Ibeas E, Hernández M, Ruiz-Gutierrez V, Nieto ML. Acidic triterpenes compromise growth and survival of astrocytoma cell lines by regulating reactive oxygen species accumulation. *Cancer Res* 2007;**67**:3741−51.
20. Moffat JG, Vincent F, Lee JA, Eder J, Prunotto M. Opportunities and challenges in phenotypic drug discovery: an industry perspective. *Nat Rev Drug Discov* 2017;**16**:531−43.
21. Dominguez E, Galmozzi A, Chang JW, Hsu KL, Pawlak J, Li W, et al. Integrated phenotypic and activity-based profiling links Ces3 to obesity and diabetes. *Nat Chem Biol* 2014;**10**:113−21.
22. Burdine L, Kodadek T. Target identification in chemical genetics: the (often) missing link. *Chem Biol* 2004;**11**:593−7.
23. Lee J, Bogyo M. Target deconvolution techniques in modern phenotypic profiling. *Curr Opin Chem Biol* 2013;**17**:118−26.
24. Parker CG, Pratt MR. Click chemistry in proteomic investigations. *Cell* 2020;**180**:605−32.
25. Niphakis MJ, Lum KM, Cognetta 3rd AB, Correia BE, Ichu TA, Olucha J, et al. A global map of lipid-binding proteins and their ligandability in cells. *Cell* 2015;**161**:1668−80.
26. Li BX, Chen J, Chao B, David LL, Xiao X. Anticancer pyrroloquinazoline LBL1 targets nuclear lamins. *ACS Chem Biol* 2018;**13**:1380−7.
27. Carelli JD, Sethofer SG, Smith GA, Miller HR, Simard JL, Merrick WC, et al. Ternatin and improved synthetic variants kill cancer cells by targeting the elongation factor-1a ternary complex. *eLife* 2015;**4**:e10222.
28. Pan S, Jang SY, Wang D, Liew SS, Li Z, Lee JS, et al. A suite of "minimalist" photo-crosslinkers for live-cell imaging and chemical proteomics: case study with BRD4 inhibitors. *Angew Chem Int Ed Engl* 2017;**56**:11816−21.
29. Conway LP, Jadhav AM, Homan RA, Li W, Rubiano JS, Hawkins R, et al. Evaluation of fully-functionalized diazirine tags for chemical proteomic applications. *Chem Sci* 2021;**12**:7839−47.
30. Li BX, Chen J, Chao B, Zheng Y, Xiao X. A lamin-binding ligand inhibits homologous recombination repair of DNA double-strand breaks. *ACS Cent Sci* 2018;**4**:1201.
31. Xiao X, Li BX. Identification of lamins as the molecular targets of LBL1 using a clickable photoaffinity probe. *Methods Enzymol* 2020;**633**:185−201.
32. Guo H, Xu J, Hao P, Ding K, Li Z. Competitive affinity-based proteome profiling and imaging to reveal potential cellular targets of betulinic acid. *Chem Commun (Camb)* 2017;**53**:9620−3.
33. Church RFR, Kende AS, Weiss MJ, Diazirines I. Some observations on the scope of the ammonia-hydroxylamine-*O*-sulfonic acid diaziridine synthesis. The preparation of certain steroid diaziridines and diazirines. *J Am Chem Soc* 1965;**87**:2665−71.
34. Church RFR, Weiss MJ. Diazirines. II. Synthesis and properties of small functionalized diazirine molecules. Observations on the reaction of a diaziridine with the iodine-iodide ion system. *J Org Chem* 1970;**35**:2465−71.
35. Wang L, Tachrim ZP, Kurokawa N, Ohashi F, Sakihama Y, Hashidoko Y, et al. Base-mediated one-pot synthesis of aliphatic diazirines for photoaffinity labeling. *Molecules (Basel, Switzerland)* 2017;**22**:1389.
36. Wang L, Ishida A, Hashidoko Y, Hashimoto M. Dehydrogenation of the NH–NH bond triggered by potassium *tert*-butoxide in liquid ammonia. *Angew Chem Int Ed Engl* 2017;**56**:870−3.
37. Murai Y, Masuda K, Sakihama Y, Hashidoko Y, Hatanaka Y, Hashimoto M. Comprehensive synthesis of photoreactive (3-trifluoromethyl)diazirinyl indole derivatives from 5- and 6- trifluoroacetylindoles for photoaffinity labeling. *J Org Chem* 2012;**77**:8581−7.
38. Haberkant P, Raijmakers R, Wildwater M, Sachsenheimer T, Brugger B, Maeda K, et al. *In vivo* profiling and visualization of cellular protein–lipid interactions using bifunctional fatty acids. *Angew Chem Int Ed Engl* 2013;**52**:4033−8.
39. Hoffmann JE, Dziuba D, Stein F, Schultz C. A bifunctional noncanonical amino acid: synthesis, expression, and residue-specific proteome-wide incorporation. *Biochemistry* 2018;**57**:4747−52.
40. Yang T, Liu Z, Li XD. Developing diazirine-based chemical probes to identify histone modification 'readers' and 'erasers. *Chem Sci* 2015;**6**:1011−7.
41. Li Z, Hao P, Li L, Tan CY, Cheng X, Chen GY, et al. Design and synthesis of minimalist terminal alkyne-containing diazirine photo-crosslinkers and their incorporation into kinase inhibitors for cell- and tissue-based proteome profiling. *Angew Chem Int Ed Engl* 2013;**52**:8551−6.
42. Suman P, Patel A, Solano L, Jampana G, Gardner ZS, Holt CM, et al. Synthesis and cytotoxicity of baylis-hillman template derived betulinic acid-triazole conjugates. *Tetrahedron* 2017;**73**:4214−26.
43. Barton DHR, O'Brien RE, Sternhell S. A new reaction of hydrozones. *J Chem Soc* 1962:470−6.
44. Barton DHR, Bashiardes G, Fourrey JL. An improved preparation of vinyl iodides. *Tetrahedron Lett* 1983;**24**:1605−8.
45. Xie F, Li BX, Kassenbrock A, Xue C, Wang X, Qian DZ, et al. Identification of a potent inhibitor of CREB-mediated gene transcription with efficacious *in vivo* anticancer activity. *J Med Chem* 2015;**58**:5075−87.
46. Schevzov G, Whittaker SP, Fath T, Lin JJ, Gunning PW. Tropomyosin isoforms and reagents. *BioArchitecture* 2011;**1**:135−64.
47. Behrmann E, Muller M, Penczek PA, Mannherz HG, Manstein DJ, Raunser S. Structure of the rigor actin–tropomyosin–myosin complex. *Cell* 2012;**150**:327−38.
48. Martinez Molina D, Jafari R, Ignatushchenko M, Seki T, Larsson EA, Dan C, et al. Monitoring drug target engagement in cells and tissues using the cellular thermal shift assay. *Science* 2013;**341**:84−7.
49. Liu HP, Bretscher A. Purification of tropomyosin from saccharomyces cerevisiae and identification of related proteins in schizosaccharomyces and physarum. *Proc Natl Acad Sci U S A* 1989;**86**:90−3.
50. Eng JK, Jahan TA, Hoopmann MR. Comet: an open-source MS/MS sequence database search tool. *Proteomics* 2013;**13**:22−4.
51. Wilmarth PA, Riviere MA, David LL. Techniques for accurate protein identification in shotgun proteomic studies of human, mouse, bovine, and chicken lenses. *J Ocul Biol Dis Infor* 2009;**2**:223−34.
52. Keller A, Nesvizhskii AI, Kolker E, Aebersold R. Empirical statistical model to estimate the accuracy of peptide identifications made by MS/MS and database search. *Anal Chem* 2002;**74**:5383−92.